

Momentum-dependent anisotropy of the charge density wave gap in quasi-1D $ZrTe_{3-x}Se_x$ (x = 0.015)

Renjie Zhang(张任杰), Yudong Hu(胡裕栋), Yiwei Cheng(程以伟), Yigui Zhong(钟益桂), Xuezhi Chen(陈学智), Junqin Li(李俊琴), Kozo Okazaki, Yaobo Huang(黄耀波), Tian Shang(商恬), Shifeng Jin(金士锋), Baiqing Lv(吕佰晴), and Hong Ding(丁洪)

Citation: Chin. Phys. B, 2025, 34 (**7**): 077106. DOI: 10.1088/1674-1056/addcc5
http://cpb.iphy.ac.cn; http://iopscience.iop.org/cpb

What follows is a list of articles you may be interested in

Competing phases and suppression of superconductivity in hole-doped Hubbard model on honeycomb lattice

Hao Zhang(张浩), Shaojun Dong(董少钧), and Lixin He(何力新)
Chin. Phys. B, 2025, 34 (**7**): 077102. DOI: 10.1088/1674-1056/adcb20

Observation of a long-range unidirectional charge density wave in kagome superconductor KV_3Sb_5

Xingwei Shi(石兴伟), Xiao Liu(刘潇), Geng Li(李更), Zhen Zhao(赵振), Haitao Yang(杨海涛), Xiao Lin(林晓), and Hong-Jun Gao(高鸿钧)
Chin. Phys. B, 2025, 34 (**7**): 077101. DOI: 10.1088/1674-1056/add7ad

The de Haas-van Alphen quantum oscillations in the kagome metal $RbTi_3Bi_5$

Zixian Dong(董自仙), Lei Shi(石磊), Bin Wang(王彬), Mengwu Huo(霍梦五), Xing Huang(黄星), Chaoxin Huang(黄潮欣), Peiyue Ma(马培跃), Yunwei Zhang(张云蔚), Bing Shen(沈冰), and Meng Wang(王猛)
Chin. Phys. B, 2024, 33 (**10**): 107102. DOI: 10.1088/1674-1056/ad6a0a

Electronic states of domain walls in commensurate charge density wave ground state and mosaic phase in 1T-TaS_2

Yan Li(李彦), Yao Xiao(肖遥), Qi Zheng(郑琦), Xiao Lin(林晓), Li Huang(黄立), and Hong-Jun Gao(高鸿钧)
Chin. Phys. B, 2023, 32 (**7**): 077101. DOI: 10.1088/1674-1056/accd4f

Flat band in hole-doped transition metal dichalcogenide observed by angle-resolved photoemission spectroscopy

Zilu Wang(王子禄), Haoyu Dong(董皓宇), Weichang Zhou(周伟昌), Zhihai Cheng(程志海), and Shancai Wang(王善才)
Chin. Phys. B, 2023, 32 (**6**): 067103. DOI: 10.1088/1674-1056/acc7f9

RAPID COMMUNICATION

Momentum-dependent anisotropy of the charge density wave gap in quasi-1D $ZrTe_{3-x}Se_x$ ($x = 0.015$)

Renjie Zhang(张任杰)[1,2,†], Yudong Hu(胡裕栋)[3,†], Yiwei Cheng(程以伟)[4,3,†], Yigui Zhong(钟益桂)[5], Xuezhi Chen(陈学智)[4,3], Junqin Li(李俊琴)[4], Kozo Okazaki[5], Yaobo Huang(黄耀波)[4], Tian Shang(商恬)[6], Shifeng Jin(金士锋)[1,2], Baiqing Lv(吕佰晴)[9,3,7,8,‡], and Hong Ding(丁洪)[3,10,11]

[1] *Beijing National Laboratory for Condensed Matter Physics and Institute of Physics, Chinese Academy of Sciences, Beijing* 100190, *China*
[2] *University of Chinese Academy of Sciences, Beijing* 100049, *China*
[3] *Tsung-Dao Lee Institute, Shanghai Jiao Tong University, Shanghai* 200240, *China*
[4] *Shanghai Synchrotron Radiation Facility, Shanghai Advanced Research Institute, Chinese Academy of Sciences, Shanghai* 201204, *China*
[5] *The Institute for Solid State Physics, The University of Tokyo, Chiba* 277–8581, *Japan*
[6] *Key Laboratory of Polar Materials and Devices (MOE), School of Physics and Electronic Science, East China Normal University, Shanghai* 200241, *China*
[7] *School of Physics and Astronomy, Shanghai Jiao Tong University, Shanghai* 200240, *China*
[8] *Zhangjiang Institute for Advanced Study, Shanghai Jiao Tong University, Shanghai* 200240, *China*
[9] *Shanghai Research Center for Quantum Sciences, Shanghai* 201315, *China*
[10] *Hefei National Laboratory, Hefei* 230088, *China*
[11] *New Cornerstone Science Laboratory, Shanghai* 201210, *China*

(Received 25 April 2025; revised manuscript received 21 May 2025; accepted manuscript online 23 May 2025)

The charge density wave (CDW) state is a ubiquitous ordered phase in condensed matter systems, characterized by a periodic modulation of the electronic charge density. In many CDW materials, superconductivity (SC) emerges in close proximity to, or coexists with, the CDW phase, offering a valuable platform to explore the interplay between these two competing orders. The $ZrTe_{3-x}Se_x$ family provides an ideal system for investigating this interplay, as both CDW-dominated and superconductivity-dominated end members have been well studied, while the intermediate compositions remain largely unexplored. In this study, we employ high-resolution angle-resolved photoemission spectroscopy (ARPES) to systematically investigate the band structure and CDW gap in Se-doped $ZrTe_{3-x}Se_x$ ($x = 0.015$), a prototypical system exhibiting the coexistence of CDW and superconductivity phases. Detailed analysis of the band structure across the Brillouin zone reveals highly momentum-dependent, anisotropic CDW gaps. Quasi-2D Fermi surface centered at $\bar{\Gamma}$ exhibits the absence of CDW gap, while on quasi-1D Fermi surface along the Brillouin zone boundary, there is also a highly anisotropic distribution of CDW gap. The gap is zero at $\bar{B}$, while reaching its maximum at a nesting vector consistent with the bulk CDW modulation. These results provide direct evidence that quasi-1D Fermi surface nesting is the primary driving force behind CDW formation in this compound. Notably, our measurements reveal a strongly suppressed density of state around E_F even out of CDW gap and absence of band folding induced by Fermi surface nesting. This observation suggests that selenium doping enhances fluctuations of the CDW order parameter, thereby weakening the long-range CDW coherence. Such enhanced fluctuations are likely to facilitate SC pairing, contributing to the observed increase in the SC transition temperature of the doped samples. Our findings not only provide comprehensive understanding of the CDW state in the $ZrTe_{3-x}Se_x$ family but also demonstrate that chemical doping provides an effective route to tune the competition between CDW and superconductivity.

Keywords: charge density wave, superconductivity, angle-resolved photoemission spectroscopy, $ZeTe_{3-x}Se_x$

PACS: 71.45.Lr, 79.60.–i, 71.55.–i, 71.20.–b

DOI: 10.1088/1674-1056/addcc5 **CSTR:** 32038.14.CPB.addcc5

1. Introduction

The charge density wave (CDW) state constitutes a ubiquitous ordered phase in condensed matter systems.[1] Contemporary theoretical frameworks attribute the emergence of CDWs to three primary mechanisms: Fermi surface nesting, electron–phonon coupling, and electron–electron correlations. Among these, CDWs driven by Fermi surface nesting are predominantly found in low-dimensional systems. Representative examples include quasi-1D compounds such as $Lu_5Ir_4Si_{10}$[2] and Ba_3TiTe_5,[3] as well as kagome metals like CsV_3Sb_5.[4] In such systems, CDW formation is associated with specific portions of the Fermi surface connected by a characteristic wave vector $\boldsymbol{q}$. When parallel or nearly parallel segments of the Fermi surface are nested via $\boldsymbol{q}$, the electronic suscep-

[†] These authors contributed equally to this work.
[‡] Corresponding author. E-mail: baiqing@sjtu.edu.cn

© 2025 Chinese Physical Society and IOP Publishing Ltd. All rights, including for text and data mining, AI training, and similar technologies, are reserved.

tibility is significantly enhanced, promoting strong scattering processes between nested regions. This redistribution of electronic states induces an instability, ultimately leading to the formation of a CDW through partial or complete nesting of the Fermi surface. In contrast, CDW formation in conventional 2D and 3D materials, such as transition metal dichalcogenides (TMDs) including 2H-$NbSe_2$,[5] 2H-$TaSe_2$,[6] NbS_2,[7] and 2H-TaS_2,[8] is primarily driven by electron–phonon coupling. In these systems, softening of specific phonon modes leads to lattice instabilities, often evidenced by the emergence of imaginary phonon frequencies, which in turn result in periodic structural distortions that stabilize the CDW state. Additionally, in strongly correlated electron systems, where the Coulomb repulsion energy is comparable to the kinetic energy, CDWs can arise from electronic correlations. Notable examples include various cuprate superconductors, such as $Bi_2Sr_2CaCu_2O_{8+\delta}$,[9] $Bi_2Sr_{2-x}La_xCuO_6$,[10] $HgBa_2CuO_{4+\delta}$,[11] and (Y,Nd)$Ba_2Cu_3O_{6+x}$.[12] Remarkably, in all three classes of CDW systems, a complex interplay often exists between CDW and superconducting phases. This observation highlights a profound connection between these two competing orders. The delicate balance between CDW and superconducting order parameters remains a central topic in the study of quantum materials. Therefore, a comprehensive investigation of the electronic structure in the CDW state is essential for unraveling the mechanisms that govern the competition and coexistence between CDW and superconductivity.

The ternary telluride $ZrTe_3$ is distinguished by the coexistence of CDW order and superconductivity,[13] making it a subject of considerable interest. Pronounced anomalies have been observed in both electrical resistivity and elastic modulus at the CDW transition temperature $T_{CDW} = 63$ K,[13] indicating strong coupling between electronic and lattice degrees of freedom. Momentum-resolved angle-resolved photoemission spectroscopy (ARPES) measurements support a nesting-driven CDW mechanism, revealing gap openings predominantly on quasi-1D band dispersions near the Brillouin zone (BZ) boundary.[14] These results are further corroborated by electron diffraction studies, which identify a characteristic CDW wave vector $\boldsymbol{q} = (1/14, 0, 1/3)$.[15] Consistent with these momentum-space observations, real-space scanning tunneling microscopy (STM) reveals a quasi-1D, incommensurate CDW modulation characterized by the same wave vector.[16] As demonstrated in classical systems exhibiting intertwined superconductivity and CDW, these two orders often compete. Consequently, suppressing CDW order is frequently an effective strategy for enhancing superconductivity. In $ZrTe_3$, the introduction of vacancies has been shown to effectively suppress long-range CDW order.[16,17] Early theoretical work has established that in low-dimensional systems, weak disorder can inhibit the formation of long-range CDW order.[18,19] In particular, the ubiquitous presence of Te vacancies in $ZrTe_3$ leads to strong pinning effects and disrupts CDW phase coherence, as confirmed by STM measurements. Moreover, vacancy tuning via crystal growth temperature can lower the CDW transition temperature and simultaneously enhance superconductivity.[17] The coexistence and apparent competition between CDW and superconductivity in $ZrTe_3$ position it as an ideal model system for exploring the intricate interplay between these collective phenomena in low-dimensional materials.

Recent studies have demonstrated that chemical doping is a powerful and systematic approach for tuning CDW and superconducting states in a variety of quantum materials. In particular, systematic substitution of selenium in the $ZrTe_{3-x}Se_x$ system has been shown to progressively suppress the CDW order,[20] with Se acting as a dilute impurity that enhances electron scattering and likely plays a role similar to that of Te vacancies in pinning the CDW phase. Thermal conductivity measurements have identified a CDW quantum critical point induced by Se doping, marking a critical transition in the electronic ground state.[21] Intriguingly, T_{SC} reaches a maximum of 4.4 K within the doping range $0.04 < x \leq 0.07$. Remarkably, even in compositions where bulk CDW order appears to be suppressed (e.g., $x = 0.1$), Raman spectroscopy continues to detect CDW-related phonon modes, suggesting the persistence of dynamic CDW fluctuations.[20] These fluctuations above T_{CDW} have also been observed in undoped $ZrTe_3$ through ARPES and STM studies.[14,16] Collectively, these findings underscore the complex interplay among CDW ordering, quantum criticality, and superconductivity in the $ZrTe_{3-x}Se_x$ system. Despite this progress, current band structure investigations have largely focused on either the CDW-dominated (low x) or superconductivity-dominated (high x) regimes. To date, the electronic structure of intermediate compositions in the range $x = 0.01$–0.04 remains unexplored. Furthermore, a comprehensive momentum-resolved mapping of the CDW gap across the BZ is still lacking. Addressing these gaps is essential for developing a deeper understanding of the doping-tuned evolution of collective electronic states in this material.

In this study, we present a comprehensive ARPES investigation of the electronic structure in Se-doped $ZrTe_{3-x}Se_x$ ($x = 0.015$), with the coexistence of CDW ($T_{CDW} = 55$ K) and superconducting orders ($T_{SC} = 2.6$ K). By systematically examining the momentum dependence of anisotropic CDW gaps, we elucidate the critical role of Fermi surface nesting in driving the CDW instability. Notably, our measurements reveal a significant suppression of spectral weight out of the CDW gap region and the absence of obvious nesting-induced

band folding near the E_F, implying that isoelectronic selenium substitution enhances fluctuations of the CDW order parameter, thereby weakening the CDW coherence and enhancing the competing superconductivity. Our work uncovers a delicate competition between CDW and superconductivity, demonstrating that controlled chemical doping provides an effective pathway for modulating the energy landscape of correlated electron systems.

2. Method

2.1. Single crystal synthesis and characterization

High-quality $ZrTe_{3-x}Se_x$ single crystals were grown by chemical vapor transport (CVT) with a nominal composition of $x = 0.015$. The crystal structure was characterized by single crystal x-ray diffraction (XRD). Electrical transport and magnetization measurements were performed in a physical property measurement system from Quantum Design.

2.2. Angle-resolved photoemission spectroscopy

Our high-resolution ARPES measurements were conducted at the BL09U beamline of the Shanghai Synchrotron Radiation Facility (SSRF) using a Scienta Omicron DA30L analyzer. Photon energies ranged from 20 eV to 150 eV, with the energy resolution of 10–80 meV and the angular resolution of 0.1°. The samples were cleaved *in situ* under a base pressure better than 5.0×10^{-11} Torr.

3. Results

The compound $ZrTe_{3-x}Se_x$ crystallizes in a monoclinic structure with space group $P21/m$. As illustrated in Fig. 1(a), the lattice features quasi-1D trigonal prismatic $ZrTe_6$ chains running along the crystallographic c-axis, where selenium atoms partially substitute tellurium. The crystal structure was confirmed by single-crystal XRD, as shown in Fig. 1(b). The corresponding three-dimensional BZ for $ZrTe_{3-x}Se_x$ is depicted in Fig. 1(c). To determine the basic physical properties of $ZrTe_{2.985}Se_{0.015}$, we conducted electric transport and magnetic susceptibility measurements. Temperature-dependent resistivity measurements reveal two distinct phase transitions (Fig. 1(d)): a CDW transition at $T_{CDW} = 55$ K, and a superconducting transition at $T_{SC} = 2.6$ K, which exceeds the superconducting transition temperature of undoped $ZrTe_3$ ($T_{SC} < 2$ K). Notably, the superconducting volume fraction of $ZrTe_{2.985}Se_{0.015}$ is nearly 100%, strongly demonstrating the nature of the bulk superconductivity (inset of Fig. 1(d)).

To elucidate the electronic band structure of $ZrTe_{3-x}Se_x$ ($x = 0.015$), we conducted systematic ARPES measurements. As shown in Fig. 2(a), photon-energy-dependent ARPES data exhibit negligible dispersion along the k_z direction, consistent with the weak interlayer coupling characteristic of van der Waals materials. This observation confirms the quasi-2D nature of the electronic structure in $ZrTe_{3-x}Se_x$.

Having established the quasi-2D nature of $ZrTe_{3-x}Se_x$, we next examined its in-plane electronic structure. Near the center of the BZ, $\bar{\Gamma}$, ARPES measurements reveal a hole-like Fermi pocket, along with an additional hole-like band located just below E_F, as shown in Fig. 2(b). Furthermore, quasi-1D electron-like Fermi surface sheets are observed along the BZ boundary. A closer inspection along the $\bar{B}$–$\bar{D}$ direction reveals two distinct electron pockets (highlighted by white dashed curves in Fig. 2(b)), which are attributed to the two inequivalent Te atoms in the unit cell. This Fermi surface splitting is consistent with previously reported features in pristine $ZrTe_3$,[22] indicating that the essential band topology is retained upon Se doping. The structural inequivalence is further corroborated by the observed splitting of the Te $4d_{3/2}$ and $4d_{5/2}$ core levels, as shown in Fig. 2(c). The absence of detectable Se-related core-level signals is expected given the low doping concentration, and suggests that Se atoms behave as dilute impurities within the lattice. To further confirm that the band structure is not significantly altered by Se doping, we compare $ZrTe_{2.985}Se_{0.015}$ and $ZrTe_{2.960}Se_{0.040}$. As shown in Figs. 3(a) and 3(d), the overall band structure remains largely unchanged upon light Se doping. The energy distribution curves (EDCs) at $\bar{\Gamma}$ and $\bar{B}$ [Figs. 3(c) and 3(d)] also exhibit no significant differences, consistent with previous reports.[23] Collectively, these observations confirm that the fundamental structural and electronic properties of $ZrTe_3$ are largely preserved in $ZrTe_{3-x}Se_x$, despite the isoelectronic substitution of Se at Te sites.

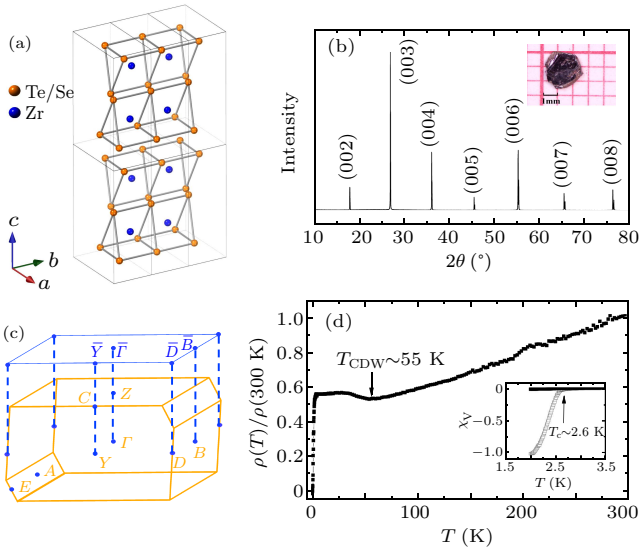


Fig. 1. The lattice structure, Brillouin zone, and basic physical characterization of $ZrTe_{3-x}Se_x$. (a) Schematic illustration of the crystal structure of $ZrTe_{3-x}Se_x$. (b) Single-crystal XRD pattern of $ZrTe_{3-x}Se_x$. (c) Three-dimensional Brillouin zone and the corresponding surface projected Brillouin zone. (d) Temperature-dependent resistivity $\rho(T)$ of $ZrTe_{0.985}Se_{0.015}$. Inset: Temperature-dependent magnetic susceptibility.

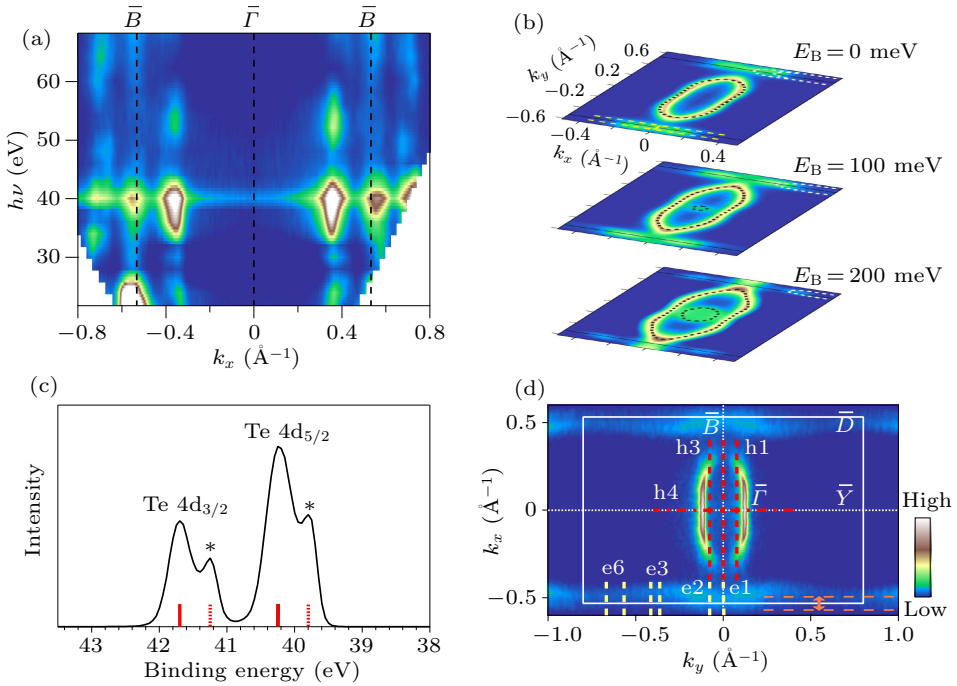


Fig. 2. Overall electronic structure of $ZrTe_{2.985}Se_{0.015}$. (a) Photon-energy-dependent Fermi surface map of $ZrTe_{2.985}Se_{0.015}$ along $\bar{B}$–$\bar{\Gamma}$–$\bar{B}$ direction. (b) Constant energy map at selective binding energies (measured with $h\nu = 38$ eV, LH). The black dashed curves mark the hole pockets centered at $\bar{\Gamma}$, while white dashed curves highlight the electron pockets along $\bar{B}$–$\bar{D}$, yellow dashed lines indicate the ideal nesting Fermi surfaces and yellow arrows highlight the nesting vector $\sim 1/14\boldsymbol{a}^*$. (c) Te $4d_{3/2}$ and $4d_{5/2}$ core-level spectrum. Asterisks indicate the splitting of the Te 4d peaks attributed to the presence of two inequivalent Te sites in the lattice, as illustrated in the inset. (d) Fermi surface of $ZrTe_{2.985}Se_{0.015}$ in the surface BZ (measured with $h\nu = 60$ eV, LH). Red and yellow dashed lines denote the momentum cuts corresponding to the ARPES spectra presented in Figs. 3 and 4, respectively. Orange dashed lines and the arrow indicate the Fermi surface nesting positions and nesting vector, respectively.

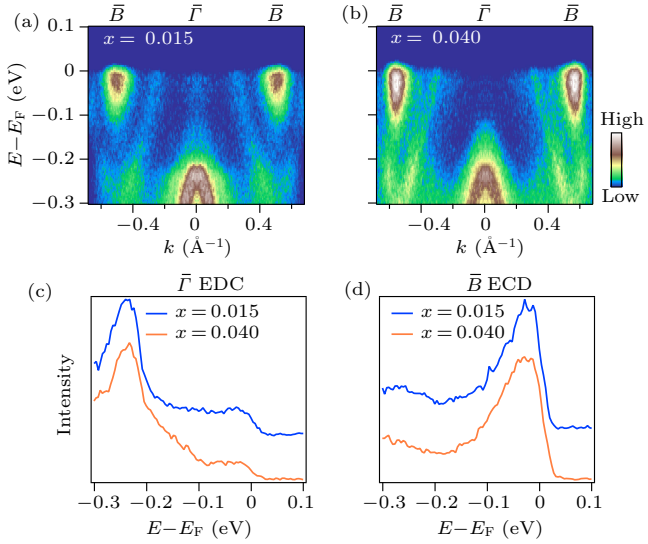


Fig. 3. Comparison of the band structure along $\bar{B}$–$\bar{\Gamma}$–$\bar{B}$ between $ZrTe_{2.985}Se_{0.015}$ and $ZrTe_{2.960}Se_{0.40}$. (a), (b) ARPES spectra along $\bar{B}$–$\bar{\Gamma}$–$\bar{B}$ for $ZrTe_{2.985}Se_{0.015}$ (a) and $ZrTe_{2.960}Se_{0.40}$ (b). Data in (a)–(d) were measured using He Iα light from a helium discharge lamp. (c), (d) EDCs, taken at $\bar{\Gamma}$ (c) and $\bar{B}$ (d), for $ZrTe_{2.985}Se_{0.015}$ (blue lines) and $ZrTe_{2.960}Se_{.40}$ (orange lines).

To further probe the mechanism underlying CDW formation in $ZrTe_{3-x}Se_x$, we systematically examined the electronic band structure along multiple momentum cuts in the BZ to identify potential CDW energy gaps. Figures 4(a)–4(d) present the ARPES band dispersions near the quasi-2D hole-type Fermi surface at the $\bar{\Gamma}$ point, measured along the momentum cuts marked by red dashed lines h1–h4 in Fig. 2(d). To minimize the influence of the Fermi–Dirac cutoff, all raw spectral data were divided by the Fermi–Dirac distribution function. Careful analysis of Figs. 4(a)–4(d) reveals that the electronic bands cross the E_F without any discernible gap opening. This finding is further substantiated by the symmetrized EDCs shown in Figs. 4(e)–4(h), which exhibit no characteristic features indicative of CDW-induced gap formation in this region of momentum space. These combined observations demonstrate that no detectable CDW gap is present on the prominent quasi-2D bands near $\bar{\Gamma}$, suggesting that the CDW order predominantly affects other regions of the Fermi surface.

Having confirmed the absence of a CDW gap on the quasi-2D hole pocket near $\bar{\Gamma}$, we turned our attention to the quasi-1D Fermi surface along the Brillouin zone boundary $\bar{B}$–$\bar{D}$. To quantitatively investigate the CDW gap formation, we performed momentum-resolved measurements along the $\bar{B}$–$\bar{D}$ symmetry line, as indicated by the yellow dashed lines e1–e6 in Fig. 2(d). Figures 5(a)–5(f) display the corresponding ARPES spectra, divided by the Fermi–Dirac distribution function, which reveal two key features: the absence of a CDW gap at $\bar{B}$ and a pronounced suppression of the density of states (DOS) near the E_F at momenta away from $\bar{B}$. These results provide direct evidence for anisotropic CDW gap opening along the quasi-1D Fermi surface.

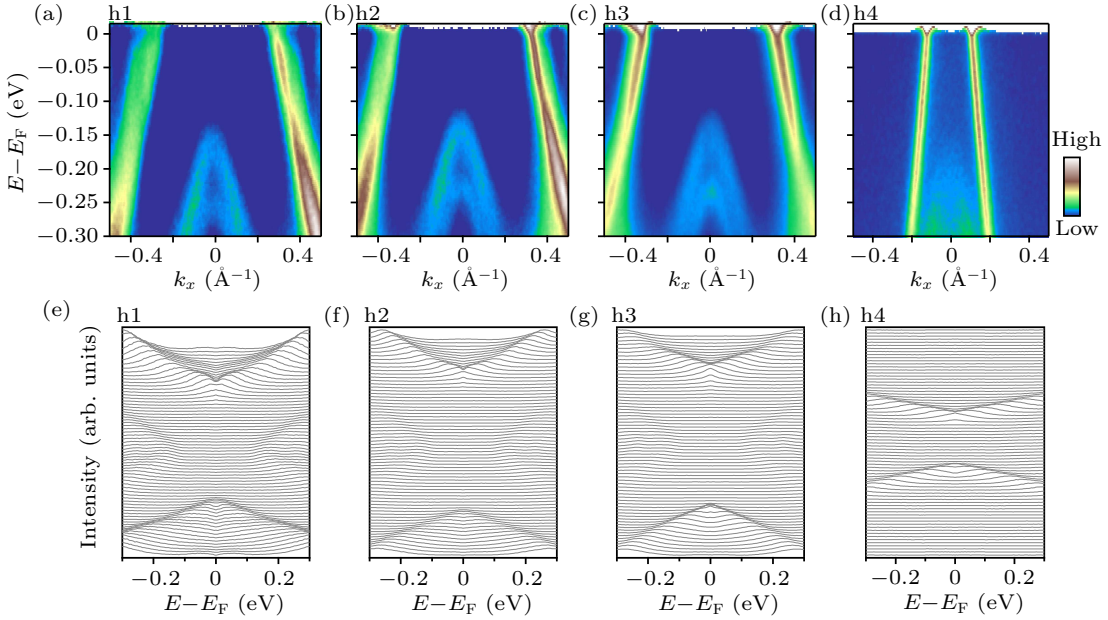


Fig. 4. ARPES spectra of the quasi-2D hole pockets. (a)–(d) ARPES intensity plot, along h1–h4 cuts indicated in Fig. 2(d), divided by Fermi–Dirac distribution function. Data in (a)–(c) were measured using 38 eV LH light; (d) was measured using 60 eV LH light. (e)–(f) Symmetrized EDCs taken from (a)–(d).

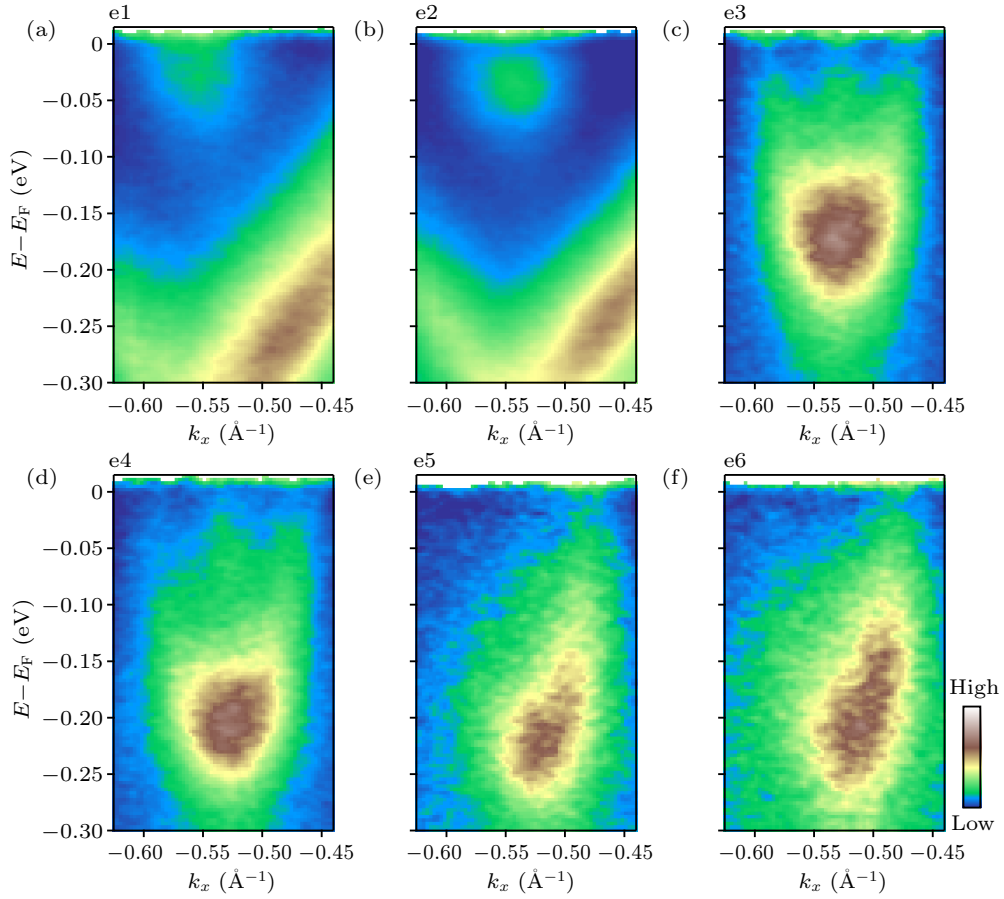


Fig. 5. ARPES spectra of the quasi-1D electron pockets along $\bar{B}$–$\bar{D}$ direction. (a)–(f) ARPES intensity plots along momentum cuts e1–e6, as indicated in Fig. 2(d), shown after division by the Fermi–Dirac distribution function to enhance visibility near the E_F. Data from (a)–(f) were measured using 38 eV LH light.

To further elucidate the anisotropic nature of the gap and quantitatively determine its magnitude, we performed a detailed analysis of the symmetrized EDCs. The symmetrized EDCs, present in Fig. 6, along the $\bar{B}$–$\bar{D}$ direction exhibit a clear momentum-dependent variation in gap size, providing direct evidence for an anisotropic CDW gap in $ZrTe_{3-x}Se_x$. The maximum gap amplitude, approximately 51 meV, is observed at cut e5, where the nesting vector $\boldsymbol{q}$ connecting segments of

the Fermi surface is $\sim 0.068\boldsymbol{a}^*$ ($\boldsymbol{a}^* = 2\pi/a$), closely aligning with the reported CDW modulation wave vector along the a^* direction ($\sim 1/14\boldsymbol{a}^*$). In contrast, at the high-symmetry point $\bar{B}$ both the Fermi–Dirac-divided spectra and the symmetrized EDCs show no discernible gap opening. This absence is attributed to the van Hove singularity near E_F, which results in a nesting vector $\boldsymbol{q} \approx 0$.[22,23] Interestingly, we also observe a substantial suppression of spectral weight along the quasi-1D Fermi surface, even outside the gapped region, extending over an energy range of approximately 100 meV near E_F. Moreover, no clear signatures of band folding, typically associated with Fermi surface nesting, are detected. These observations suggest that additional effects such as impurity-induced electronic scattering may play a significant role in modifying the CDW coherence and spectral features.[23]

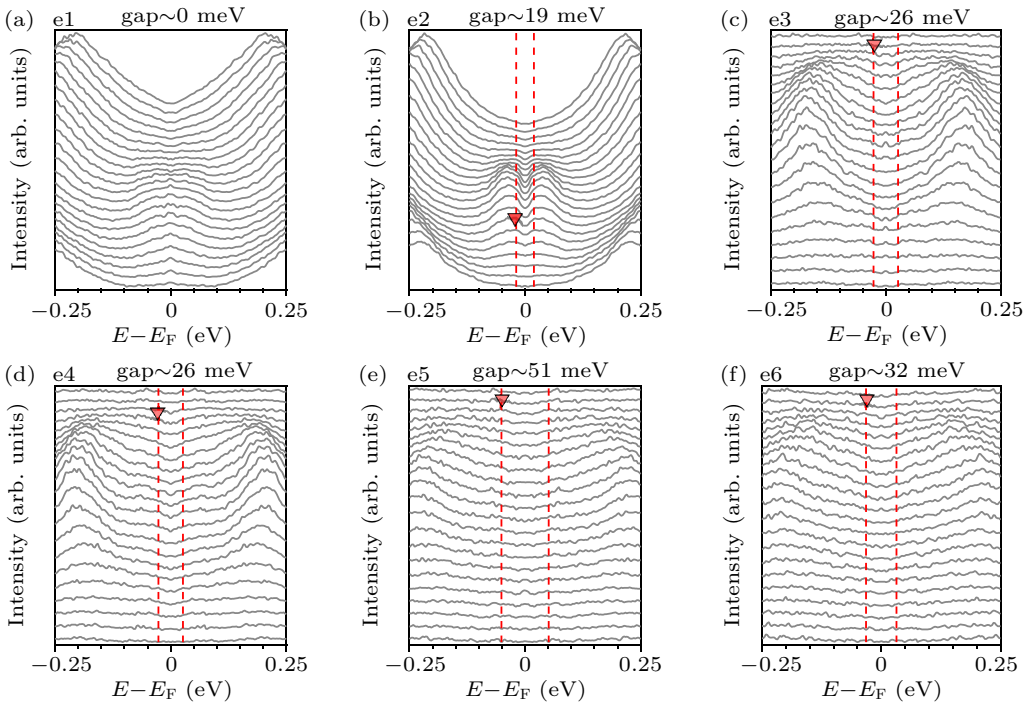


Fig. 6. Symmetrized EDCs of the quasi-1D electron pockets spectra along $\bar{B}$–$\bar{D}$ direction. (a)–(f) Symmetrized EDCs extracted from the ARPES spectra along momentum cuts e1–e6, as defined in Fig. 2(d). The red dashed lines and triangles indicate the CDW gap position.

4. Discussion

Through a systematic momentum-resolved characterization of the CDW gap across the BZ of $ZrTe_{2.985}Se_{0.015}$, our analysis confirms that the CDW formation is primarily driven by quasi-1D Fermi surface nesting. The extracted nesting vector is consistent with earlier diffraction studies,[15] reinforcing the nesting-driven nature of the CDW instability in this material.

Despite this correspondence, several notable deviations from the conventional Fermi surface nesting picture are observed: (1) a substantial suppression of the DOS near the E_F, extending across an energy window of approximately 100 meV, even outside the identified CDW gap region; and (2) the absence of clear band folding typically associated with nesting-induced CDW states. Previous studies[23] have shown that dilute Se substitution significantly enhances electronic scattering, which likely accounts for the pronounced DOS suppression near E_F. Such enhanced scattering can disrupt long-range CDW coherence, thereby suppressing the formation of well-defined folded bands in momentum space.

It is worth noting that even in undoped $ZrTe_3$, no prominent band folding has been observed. STM studies[16] have reported the ubiquitous presence of Te vacancies in pristine $ZrTe_3$, which induce short-range CDW fluctuations persisting well above the CDW transition temperature. These findings suggest that strong electronic scattering, whether from intrinsic vacancies or extrinsic dopants, plays a critical role in modulating CDW coherence throughout the $ZrTe_{3-x}Se_x$ system.

Crucially, we emphasize the strong interplay between CDW order and superconductivity in $ZrTe_{3-x}Se_x$. Whether by intercalating $ZrTe_3$ with Ni/Cu[24–26] or by reducing its thickness via exfoliation,[27] both approaches reveal a clear anti-correlation between superconductivity and CDW, underscoring the competitive relationship between these two electronic phases. Since the CDW in this system is primarily driven by Fermi surface nesting, the observed anisotropic superconductivity likely originates, at least in part, from the quasi-1D Fermi surface. Indeed, by systematically controlling the vacancy concentration[17] through varying the crystal growth temperature, upper critical field measurements indicate that the bulk and filamentary superconducting components are associated with the quasi-2D and quasi-1D Fermi pockets, respectively. Once the CDW develops, it suppresses the density of states at the DOS at E_F — as evidenced by our experiments

— thereby disfavoring superconductivity on the same quasi-1D Fermi surface.[28] In contrast, Se doping or increasing Te vacancies suppresses long-range CDW order and consequently promotes superconductivity, highlighting the need for further investigation into the delicate balance between these competing electronic states.

5. Conclusions

In summary, we have characterized the electronic band structure of Se-doped $ZrTe_{3-x}Se_x$ ($x = 0.015$), which exhibits a CDW transition at $T_{CDW} = 55$ K and a superconducting transition at $T_{SC} = 2.6$ K, using ARPES. The system displays a mixture of two-dimensional bulk states and quasi-1D chain-like electronic features near the BZ boundary — consistent with observations in both CDW-dominated $ZrTe_3$ and superconductivity-dominated $ZrTe_{0.96}Se_4$. Core-level spectroscopy of Te reveals a clear splitting of both the $4d_{3/2}$ and $4d_{5/2}$ states, indicating the presence of two inequivalent Te sites in the lattice. Momentum-resolved analysis along the $\bar{B}$–$\bar{D}$ direction reveals an anisotropic CDW gap, with the maximum gap occurring between $\bar{B}$ and $\bar{D}$ corresponding to a nesting vector $\boldsymbol{q} \approx 1/14\boldsymbol{a}^*$. In contrast, no gap is observed at $\bar{B}$ (where $\boldsymbol{q} \approx 0$) or on the central quasi-2D Fermi pocket. These findings support a nesting-driven CDW formation mechanism rooted in the quasi-1D Fermi surface topology. Notably, the spectral weight remains strongly suppressed even outside the primary gap region along the quasi-1D Fermi surface, and no clear band folding is detected. We attribute these features to impurity-induced electronic scattering, which is particularly pronounced in $ZrTe_{3-x}Se_x$ due to intrinsic Te vacancies and/or Se dopants. This enhanced scattering disrupts long-range CDW coherence, thereby obscuring the conventional signatures expected from a fully developed nesting-induced gap. Our findings demonstrate that chemical doping serves not only to enhance the superconducting transition temperature but also provides a tunable platform for investigating the competition between CDW order and superconductivity in low-dimensional quantum materials.

Acknowledgements

B. L. acknowledges support from the National Key R&D Program of China (Grant No. 2023YFA1407400), the National Natural Science Foundation of China (Grant No. 12374063), the Shanghai Natural Science Fund for Original Exploration Program (Grant No. 23ZR1479900), and the Cultivation Project of Shanghai Research Center for Quantum Sciences (Grant No. LZPY2024). H. D. acknowledges support from the Innovation Program for Quantum Science and Technology (Grant No. 2021ZD0302700), the New Cornerstone Science Foundation (Grant No. 23H010801236), and the National Natural Science Foundation of China (Grant No. 12488101). We acknowledge the technical support provided by the BL09U (31124.02.SSRF.BL09U) beamlines at the Shanghai Synchrotron Radiation Facility (SSRF) for conducting the ARPES measurements.

References

[1] Zhu X, Cao Y, Zhang J, Plummer E W and Guo J 2015 *Proc. Natl. Acad. Sci. USA* **112** 2367
[2] Leroux M, Mishra V, Opagiste C, Rodière P, Kayani A, Kwok W K and Welp U 2020 *Phys. Rev. B* **102** 094519
[3] Zhang J, Jia Y, Wang X, Li Z, Duan L, Li W, Zhao J, Cao L, Dai G, Deng Z, Zhang S, Feng S, Yu R, Liu Q, Hu J, Zhu J and Jin C 2019 *NPG Asia Mater.* **11** 1
[4] Ortiz B R, Teicher S M L, Kautzsch L, Sarte P M, Ratcliff N, Harter J, Ruff J P C, Seshadri R and Wilson S D 2021 *Phys. Rev. X* **11** 041030
[5] Kundu A K, Rajapitamahuni A, Vescovo E, Klimovskikh I I, Berger H and Valla T 2024 *Commun. Mater.* **5** 208
[6] Sur Y, Gim D H, Bhoi D, Jang D H, Murata K, Hu J W, Zhang K, Cao Z Y, Struzhkin V V, Chen X J and Kim K H 2025 *NPG Asia Mater.* **17** 1
[7] Heil C, Poncé S, Lambert H, Schlipf M, Margine E R and Giustino F 2017 *Phys. Rev. Lett.* **119** 087003
[8] Liu H, Huangfu S, Zhang X, Lin H and Schilling A 2021 *Phys. Rev. B* **104** 064511
[9] da Silva Neto E H, Aynajian P, Frano A, Comin R, Schierle E, Weschke E, Gyenis A, Wen J, Schneeloch J, Xu Z, Ono S, Gu G, Le Tacon M and Yazdani A 2014 *Science* **343** 393
[10] Kawasaki S, Tsukuda N, Lin C and Zheng G 2024 *Nat. Commun.* **15** 5082
[11] Tabis W, Li Y, Tacon M L, Braicovich L, Kreyssig A, Minola M, Dellea G, Weschke E, Veit M J, Ramazanoglu M, Goldman A I, Schmitt T, Ghiringhelli G, Barišić N, Chan M K, Dorow C J, Yu G, Zhao X, Keimer B and Greven M 2014 *Nat. Commun.* **5** 5875
[12] Ghiringhelli G, Tacon M L, Minola M, Blanco-Canosa S, Mazzoli C, Brookes N B, Luca G M D, Frano A, Hawthorn D G, He F, Loew T, Sala M M, Peets D C, Salluzzo M, Schierle E, Sutarto R, Sawatzky G A, Weschke E, Keimer B and Braicovich L 2012 *Science* **337** 821
[13] Takahashi S, Sambongi T, Brill J W and Roark W 1984 *Solid State Commun.* **49** 1031
[14] Yokoya T, Kiss T, Chainani A, Shin S and Yamaya K 2005 *Phys. Rev. B* **71** 140504
[15] Eaglesham D J, Steeds J W and Wilson J A 1984 *J. Phys. C: Solid State Phys.* **17** L697
[16] Liu L, Zhu C, Liu Z Y, Deng H, Zhou X B, Li Y, Sun Y, Huang X, Li S, Du X, Wang Z, Guan T, Mao H, Sui Y, Wu R, Yin J X, Cheng J G and Pan S H 2021 *Phys. Rev. Lett.* **126** 256401
[17] Nomura A, Kobayashi S, Ohta S and Sakata H 2021 *Europhys. Lett.* **133** 37003
[18] Imry Y and Ma S 1975 *Phys. Rev. Lett.* **35** 1399
[19] Sham L J and Patton B R 1976 *Phys. Rev. B* **13** 3151
[20] Zhu X, Ning W, Li L, Ling L, Zhang R, Zhang J, Wang K, Liu Y, Pi L, Ma Y, Du H, Tian M, Sun Y, Petrovic C and Zhang Y 2016 *Sci. Rep.* **6** 26974
[21] Cui S, He L P, Hong X C, Zhu X D, Petrovic C and Li S Y 2016 *Chin. Phys. B* **25** 077403
[22] Hoesch M, Cui X, Shimada K, Battaglia C, Fujimori S and Berger H 2009 *Phys. Rev. B* **80** 075423
[23] Hoesch M, Gannon L, Shimada K, Parrett B J, Watson M D, Kim T K, Zhu X and Petrovic C 2019 *Phys. Rev. Lett.* **122** 017601
[24] Lei H, Zhu X and Petrovic C 2011 *Europhys. Lett.* **95** 17011
[25] Ganose A M, Gannon L, Fabrizi F, Nowell H, Barnett S A, Lei H, Zhu X, Petrovic C, Scanlon D O and Hoesch M 2018 *Phys. Rev. B* **97** 155103
[26] Zhu X, Lei H and Petrovic C 2011 *Phys. Rev. Lett.* **106** 246404
[27] Chen X, Zhu C, Lei B, Zhuo W, Wang W, Ma J, Luo X, Xiang Z and Chen X 2024 *Phys. Rev. B* **109** 144513
[28] Rahn D J, Hellmann S, Kalläne M, Sohrt C, Kim T K, Kipp L and Rossnagel K 2012 *Phys. Rev. B* **85** 224532